



# CHALMERS

## Chalmers Publication Library

### **Microstrip-Ridge Gap Waveguide – Study of Losses, Bends and Transition to WR-15**

This document has been downloaded from Chalmers Publication Library (CPL). It is the author's version of a work that was accepted for publication in:

**IEEE transactions on microwave theory and techniques (ISSN: 0018-9480)**

Citation for the published paper:

Raza, H. ; Yang, J. ; Kildal, P. (2014) "Microstrip-Ridge Gap Waveguide – Study of Losses, Bends and Transition to WR-15". IEEE transactions on microwave theory and techniques, vol. 62(9), pp. 1943 - 1952.

<http://dx.doi.org/10.1109/TMTT.2014.2327199>

Downloaded from: <http://publications.lib.chalmers.se/publication/202890>

Notice: Changes introduced as a result of publishing processes such as copy-editing and formatting may not be reflected in this document. For a definitive version of this work, please refer to the published source. Please note that access to the published version might require a subscription.

Chalmers Publication Library (CPL) offers the possibility of retrieving research publications produced at Chalmers University of Technology. It covers all types of publications: articles, dissertations, licentiate theses, masters theses, conference papers, reports etc. Since 2006 it is the official tool for Chalmers official publication statistics. To ensure that Chalmers research results are disseminated as widely as possible, an Open Access Policy has been adopted. The CPL service is administrated and maintained by Chalmers Library.

(article starts on next page)

# Microstrip-Ridge Gap Waveguide – Study of Losses, Bends and Transition to WR-15

Hasan Raza, Jian Yang, *Senior Member, IEEE*, Per-Simon Kildal, *Fellow, IEEE*, Esperanza Alfonso, *Member, IEEE*

**Abstract**—This paper presents the design of microstrip-ridge gap waveguide using via holes in PCBs, a solution for high frequency circuits. The study includes how to define the numerical ports, pin sensitivity, losses, and also a comparison with performance of normal microstrip line and inverted microstrip lines. The results are produced using commercially available EM simulators. A WR-15 to microstrip-ridge gap waveguide transition was also designed. The results are verified with measurements on microstrip-ridge gap waveguides with WR15 transitions at both ends.

**Index Terms**— Gap Waveguide, Inverted Microstrip Line, Microstrip Line.

## I. INTRODUCTION

REALIZATION of all kinds of waveguides at high frequencies above 40 GHz is a manufacturing challenge. Mechanical tolerances become critical and limit the performance. Recently, the gap waveguide technology was introduced for making low loss circuits at millimeter and sub-millimeter waves [1]-[3], where the theoretical background was presented in [1][2] and experimental verification in [3]. There are basically three different kinds of gap waveguides that can be formed between parallel metal plates, as described in [2], i.e., groove, ridge and microstrip gap waveguides. The principle of operation is based on creating invisible magnetic walls in the form of a parallel-plate cut-off on both sides of these grooves, ridges or microstrip lines, by using quasi-periodic elements like metal pins or mushrooms as studied in [4]. The gap waveguides provide low loss propagation for designing microwave circuits, but the technology can also be used to package normal microstrip circuits [5] and active microwave modules [6]. Such packaging normally improves performance compared to the unpackaged case and packaging involving absorbers, such as demonstrated in [6] and for microstrip filters in [7]. The gap waveguide has a special advantage when packaging inverted microstrip lines [8]. Such inverted microstrip gap waveguide line is realized by having a dielectric layer over a periodic pattern of pins [2], and there is an air gap between the top metal plate and the substrate

material supporting the microstrip line. The pin structure works as an artificial magnetic surface (AMC), so the inverted microstrip gap waveguide is an AMC-packaged inverted (or suspended) microstrip line [9].

In a high-gain gap waveguide array antenna at 60 GHz we would like to realize the distribution network in gap waveguide and have slots in the smooth upper plate that couple to directive radiating elements, e.g., in the form of cavity-backed 2x2 slot arrays like in [10]. We would also like to have a transition to WR15 in the lower textured plate, for connection to the transmitting and receiving amplifiers. We can excite radiating elements over a large 15% bandwidth from inverted microstrip gap waveguide, e.g., as reported in [11]. However, we did not succeed in realizing a wideband WR15 transition to the rear side from the inverted microstrip gap waveguide, as also explained in [10], whereas we managed to do it in the present microstrip-ridge gap waveguide. Therefore, we chose the microstrip-ridge gap waveguide for the antenna in [10]. The present paper shows the design of this wideband WR15 transition, and contains in addition a theoretical and experimental study of the losses in the microstrip-ridge gap waveguide.

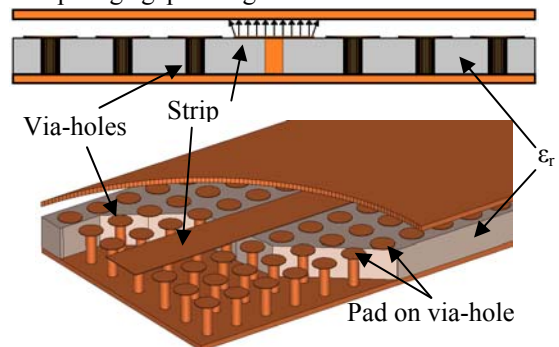


**Figure 1** Basic configuration of microstrip-ridge gap waveguide.

Thus, we are presenting here the design and demonstration of microstrip-ridge gap waveguide. This is obtained by using a substrate with ground plane and shorting the inverted microstrip line periodically by metalized via holes to this ground plane. The AMC layer is created by a periodic pattern of metalized via holes in the same substrate, like in [12]. The AMC-type via-hole surface produces together with the upper metal surface a stopband for all types of parallel-plate modes in the air gap, except for the quasi-TEM mode along the inverted microstrip line (i.e., the metal strip).

The numerical design of microstrip-ridge gap waveguides is

Hasan Raza, Jian Yang and Per-Simon Kildal are with the Dept. of signals and systems, Chalmers University of Technology. e-mail: hasan.raza, jian.yang, per-simon.kildal@chalmers.se. Esperanza Alfonso is with Gapwaves (<http://gapwaves.com>). Email: Esperanza.alfonso@gapwaves.com.

complicated because there are no ports in common EM solvers that are suitable for its specific quasi-periodic geometry [13]. Therefore, this paper also addresses how to define the numerical ports in the microstrip-ridge gap waveguide, and also a study of its sensitivity to the pin locations. We will also compare the performance of microstrip-ridge gap waveguide with normal microstrip lines and inverted microstrip lines in terms of the losses suffered by the line at 60 GHz. The calculated results in this paper are produced using CST Microwave Studio [14].

## II. GEOMETRY AND MODELING

The geometry of the microstrip-ridge gap waveguide with via holes is shown in Figure 1. The strip at the surface of the substrate is connected to the ground plane through quasi-periodic via holes. The periodic pattern of via holes in the substrate material on both sides of the microstrip line creates a PMC layer that prohibits waves from propagating in the air gap between the PCB and the upper metal plate, except for waves following the inverted microstrip line in the form of a quasi-TEM mode. The via holes work similarly to a pin surface does, with pin height of 0.508 mm and diameter 0.25 mm. The diameter of the pad at the top of the via-hole is 0.7588 mm. The distance between two vias is 1.0 mm. The substrate material is 0.508 mm thick Rogers RO3003 having  $\epsilon_r$  equal to 3.0. The air gap is 0.25 mm. The dispersion diagram determines the major characteristics of the gap waveguide. By using the Eigen mode solver in CST microwave studio, the dispersion diagram is calculated as a function of frequency for specific choices of dimensions of the gap waveguide, as shown in Figure 2a. We see that the stopband of the parallel-plate modes for this specific case is between 45 and 72 GHz and within this band only one single inverted microstrip mode is propagating.

For the case of gap waveguide realized with metallic pins, the stopband is mainly controlled by the air gap, and the height, width and period of the pins [4]. In the present case the diameter of the pads on the top of the via-hole pins, and the relative permittivity of the PCB, also affect the stopband. The pads appear due to the metallization process of the via-hole and cannot be avoided. The substrate material was chosen to be RO3003 in order to cost-effectively minimize the losses in the microstrip-ridge gap waveguide. Such losses are present even for the inverted microstrip geometry as discussed in more detail in section IV. Figure 2b shows a study summarizing the effect of the pad diameter. It can clearly be seen that, by keeping the period and via-hole diameter fixed, an increase in the pad diameter will shift the stopband toward lower frequencies.

### A. Port Definition and Simulated Results

The definition of a good numerical waveguide port for the microstrip-ridge gap waveguide is not easy, in the sense that we need to modify the via-hole under the strip in front of the port in order to make it work well. This modification was done in order to match the numerical rectangular waveguide port to the microstrip-ridge gap waveguide, as shown in Figure 3. Using Ansoft HFSS [15], we found that the available lumped

port was well matched with the microstrip-ridge gap waveguide, but the equivalent of this port in CST [14] was not working well. So, we used the rectangular waveguide port in CST and matched it by using a small finite length rectangular block just in front of the port, starting from the edge of the strip. The width of the rectangular block is the same as that of the diameter of a via hole.

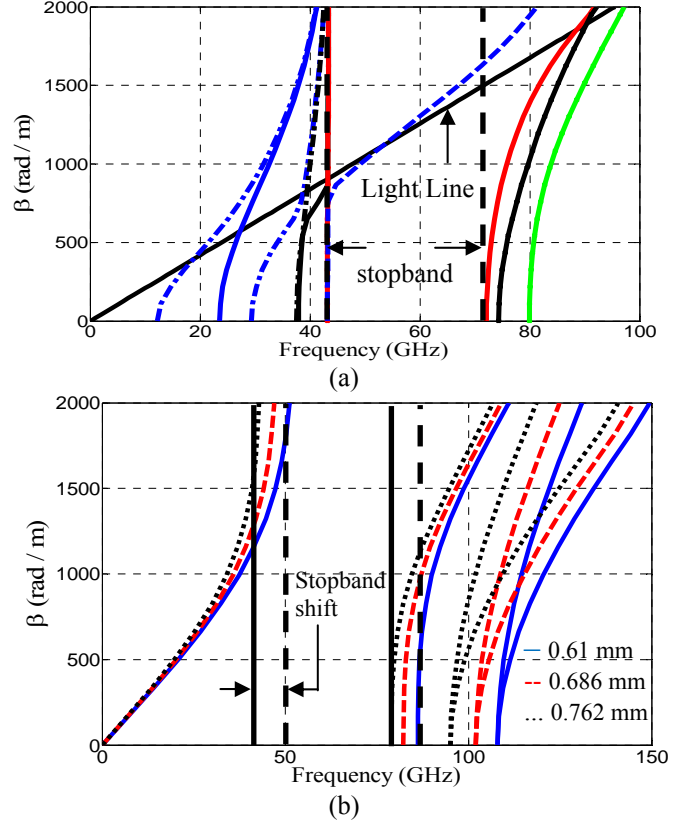


Figure 2a) Dispersion diagram of microstrip-ridge gap waveguide. b) Dispersion diagram for various pad diameters.

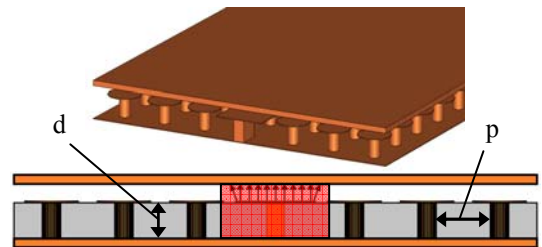
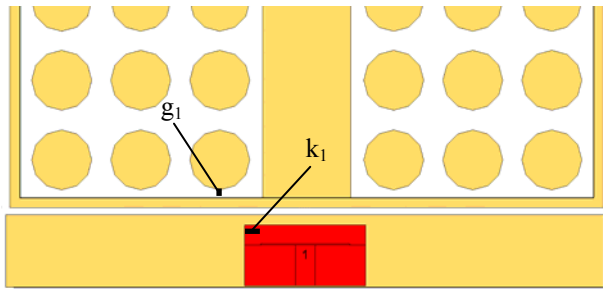


Figure 3 Port definition for the microstrip-ridge gap waveguide.

Similarly, we also did a study of the width and the location of the waveguide port relative to the first row of pins. For this purpose, we considered a straight microstrip-ridge line and connected numerical ports at both ends of it. The most important parameters for this study are shown in Figure 4. The best results are when  $k_1$  is  $4p/15$  and  $g_1$  is  $2p/15$ , where  $p$  is the spacing between two via-holes and  $d$  is the thickness of the substrate  $\epsilon_r$ , as shown in Figure 3. The criterion of the selection was the minimum reflection coefficient within the stopband. The simulated S-parameters are shown in Figure 5. It can be seen that the reflection coefficient is below -20 dB

over the desired bandwidth of 57-66 GHz, and  $S_{21}$  is about -0.2 dB. This shows that the numerical ports are reasonably well matched with the line. The transmission losses become almost twice as large if the length of the line is doubled, so there are noticeable ohmic losses in the line.

We accepted the numerical port to be good enough for designing microstrip-ridge gap waveguides using CST Microwave Studio. The port could have been better, but the results of the circuits were in the end quite good anyway. We were not able to match equally well the corresponding rectangular waveguide port in HFSS.



**Figure 4** Definition of port geometry relative to the vias and microstrip line, cross-sectional view (lower case) and top view (Upper case)

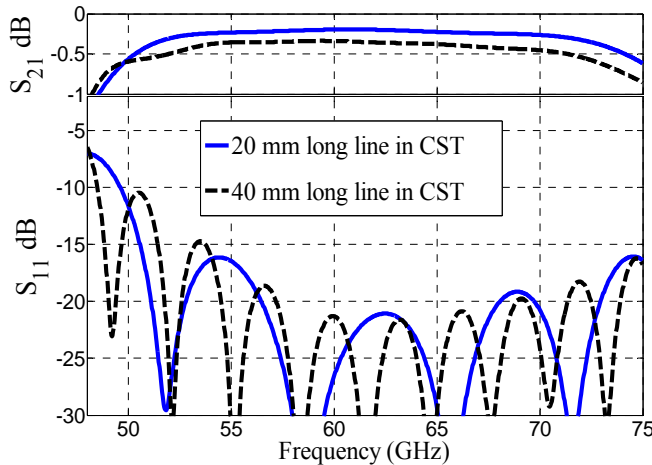


**Figure 5** Simulated S-parameters of the microstrip-ridge waveguide.

### B. Design of 90° bend

The locations of the via-holes around a 90° bend are very critical to get good performance. This is important because mechanically there is a minimum mechanical spacing which is allowed between the via-holes, determined by the manufacturing process. At the same time the via-holes at the corner of the bend must be close enough to each other to avoid any resonant cavities. This maximum spacing is known from the Eigen mode unit cell simulations. We tuned the via-hole locations inside the marked area in Figure 6, to obtain the lowest  $S_{11}$  and highest  $S_{21}$  over the whole bandwidth. Similarly, we tuned mitering of the bend (shown by the darker region of the line) in order to minimize its effect. The simulated S-parameters before and after the tuning are shown in Figure 7. Again, the final simulated  $S_{11}$  is below -20 dB over 57-66 GHz and  $S_{21}$  is about -0.2 dB.

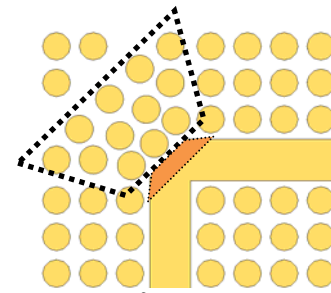


**Figure 6** Geometry of the 90° bend, with the area of tuned pins and portion of bend.

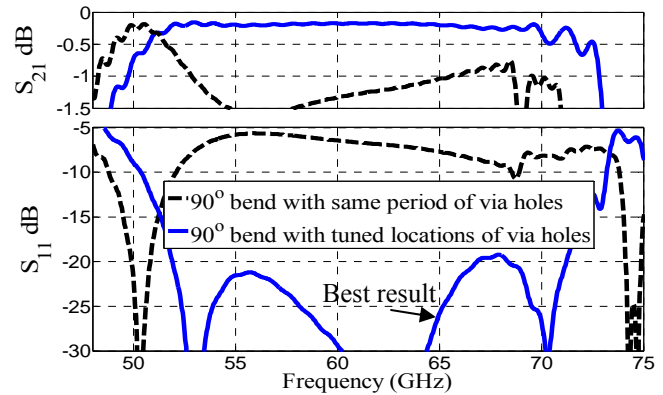


**Figure 7** Simulated S-parameters of the microstrip-ridge gap waveguide 90° bend with and without tuning of pins location at the corner and mitered bend.

### C. Sensitivity due to Via Hole Location

We show in Figure 5 the simulated  $S_{11}$  and  $S_{21}$  of a simple straight microstrip-ridge gap waveguide and of a 90° bend in Figure 7. The transmission coefficient is better than -0.3 dB over the desired frequency band whereas  $S_{11}$  is below -20dB. In this section we will discuss how sensitive the line is with respect to the displacement of the via-hole locations.

For this purpose we have considered two examples. The first example is using a straight line, and we will displace each pin in each column as shown in Figure 8. First, we displace only the first pin (nearest to the line) and the effect is shown in Figure 9a. Similarly the effect by displacing the second and third pin is also shown in Figure 9a. It can clearly be seen that the first pin has the most significant effect on the performance of line where the change in  $S_{11}$  is more than 8 dB. This effect is produced when the via is moved about 0.15 mm towards the line. The degradation is increased to 2 dB when the via is moved 0.2 mm away from the line. Similarly, by displacing the via-hole 0.2 mm along the line there will be a change of 3 dB in  $S_{11}$ .

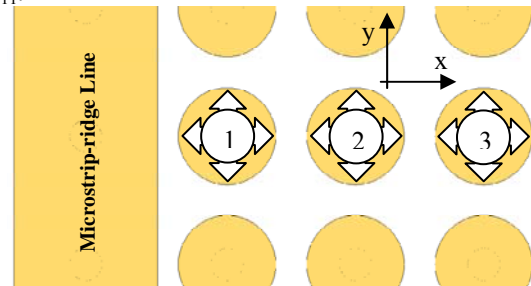


**Figure 8** Displacement of via-holes along the line.

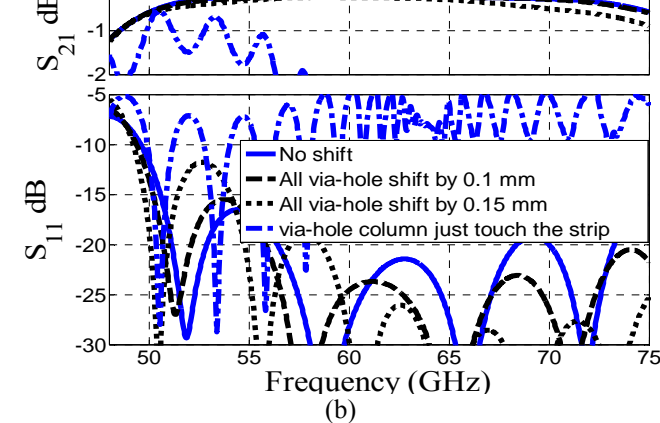
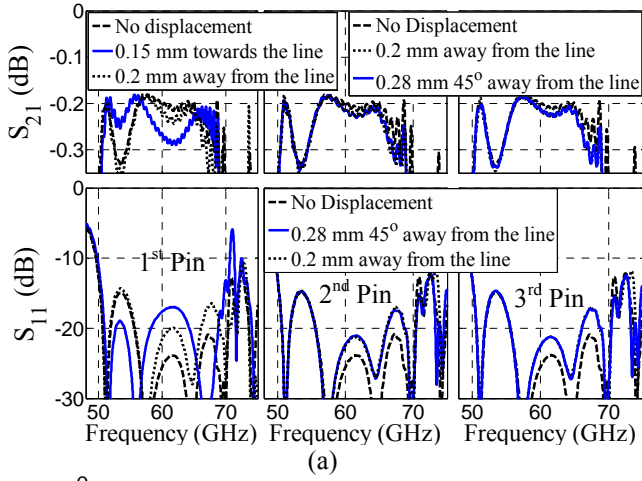


Figure 9 Variation in  $S_{11}$  and  $S_{21}$  with respect to displacement, (a) single via-hole in each column, (b) all via-holes.

The variation in  $S_{11}$  due to the second and third pin is within 3 dB when moving in different directions. Another way to look at the variations is by keeping the location of the strip fixed and displacing all the via-holes along x-axis (see Figure 8). Figure 9b show the variations in the S-parameters due to the displacement of all the via-holes. The worst case is when the pads of the via-holes touch the strip. Similarly, we have considered another example in which we displace the pins at the corner of the bend as shown in Figure 10. While realizing the  $90^\circ$  bend in microstrip-ridge gap waveguide, we found that the performance of the bend is very sensitive to the via-holes close to the bend. For this study we have selected a set of via-holes for each of the first three rows of pins at the corner of the  $90^\circ$  bend.

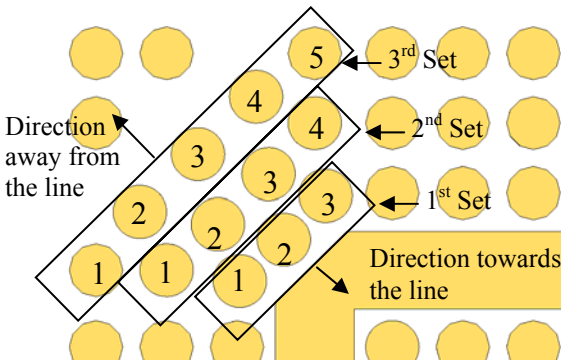


Figure 10 Displacement of via-holes at the corner of  $90^\circ$  bend.

Figure 11-13 show the variations in  $S_{11}$  and  $S_{21}$  caused by moving the pins at the bend. It can easily be observed that the middle pin in the 1<sup>st</sup> set has the most significant effect, if displaced by 0.2 mm, where the variation in  $S_{11}$  is about 20 dB. The displacement of the remaining via holes cause variation in  $S_{11}$  of 3 dB. The width of the strip is very wide in comparison with that of normal microstrip lines at these frequencies, because microstrip-type gap waveguide do not have problems with surface waves and radiation that appear in normal microstrip circuits when wide lines and thick substrates are used. The wider metal strips make the metal losses much smaller than the metal losses of narrow microstrip lines, and at high frequencies it becomes also easier to realize circuits when the metal strips are wide. The comparison of the microstrip-ridge gap waveguide with normal microstrip and inverted microstrip line will be present in the next section.

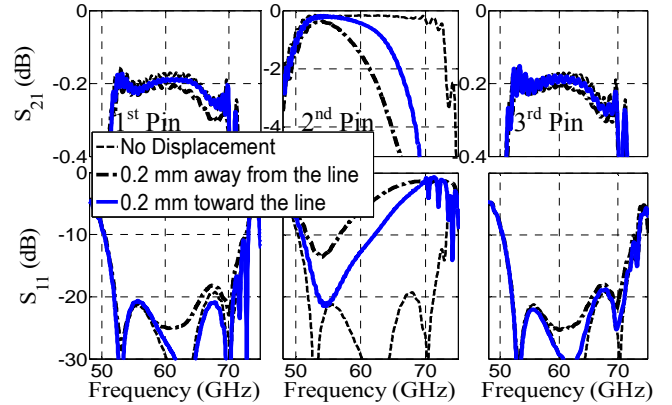


Figure 11 Variation in  $S_{11}$  and  $S_{21}$  with respect to displacement of 1<sup>st</sup> set of pins at corner of  $90^\circ$  bend.

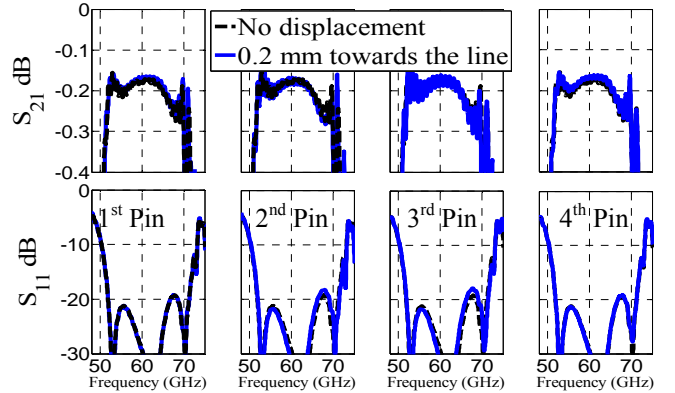
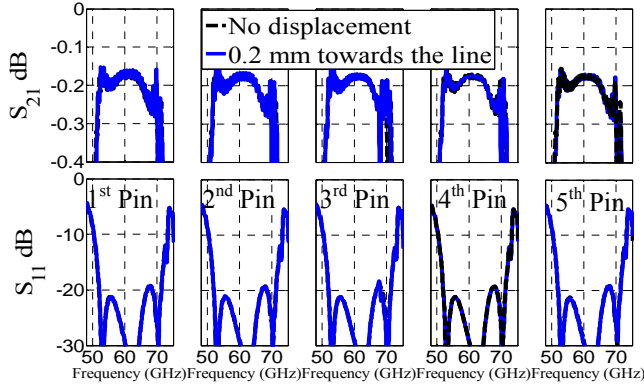


Figure 12 Variation in  $S_{11}$  and  $S_{21}$  with respect to displacement of 2<sup>nd</sup> set of pins at corner of  $90^\circ$  bend.

### III. COMPARISON BETWEEN MICROSTRIP-RIDGE GAP LINE, NORMAL MICROSTRIP LINE AND INVERTED MICROSTRIP LINE

Microstrip lines are most commonly used in microwave integrated circuits [16], besides coplanar waveguides. Microstrip line losses consist of both conductor and dielectric losses. In addition, there are radiation losses due to discontinuities (such as open circuits, short circuits and bends) and losses due to surface waves [16]. The latter is in particular large for large substrate thicknesses. The dielectric losses themselves do not depend on the thickness of the substrate and its dimensions, whereas the conductor losses reduce inversely

proportional to the line width (for constant line impedance). The conductor losses include the actual conductance of the material, the frequency dependent skin effect losses, and the losses due to the roughness of the surface (random scratches and bumps) [17]. The skin depth and overall effect of conductivity depends also on any type of protection used against the verdigris patina on copper surfaces.



**Figure 13** Variation in  $S_{11}$  and  $S_{21}$  with respect to displacement of 3<sup>rd</sup> set of pins at corner of 90° bend.

Figure 14 shows an example of the losses suffered by a 3 cm long microstrip line with two 90° bends when realized with different combinations of materials. Obviously, the best is the case when the conductor is a Perfect Electric Conductor (PEC) and the dielectric material is lossless. The “lossless” substrate cases in this and later graphs are simply modeled by setting the loss tangent of the material to zero. The transmission coefficient for this “PEC and lossless substrate” case is about -0.75 dB at 60 GHz. Since the materials are assumed to be lossless, the only contributions to the losses in this case are surface waves and radiation losses at the bends, in addition to the mismatch factor. The loss increases by 0.5 dB, if we use copper instead of PEC. This loss is much larger than the case when the dielectric become lossy and the conductor remains PEC. Together, the lossy dielectric and copper give a loss of nearly 0.75 dB everywhere within the bandwidth. This example clearly shows that the combined losses due to the conductor and the surface waves and radiation are much larger than the losses due to the dielectric at high frequencies, provided a low loss substrate like RO 3003 is used.

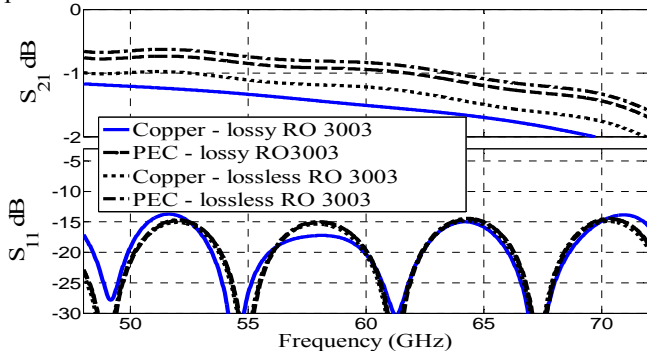


**Figure 14** S-parameters of microstrip line, with lossy/lossless conductor and lossy/lossless dielectric.

Similarly, the inverted microstrip line can be used as a low loss line [18]. Figure 15 shows the simulated  $S_{11}$  and  $S_{21}$  of a microstrip line and an inverted microstrip line of similar strip

width, air gap and length as the microstrip-ridge gap waveguide. The width of the strip, length, and air gap is 1.1176 mm, 15 mm, and 0.25 mm, respectively. It can clearly be seen that, with similar widths, the microstrip-ridge gap waveguide has much lower transmission losses. The overall losses can be reduced in microstrip line and inverted microstrip line, if we reduce the substrate thickness so that the width of the lines can be reduced by factors two and four of that of the microstrip-ridge gap waveguide, but the microstrip-ridge gap waveguide is still much better. The results are shown in Figure 16.

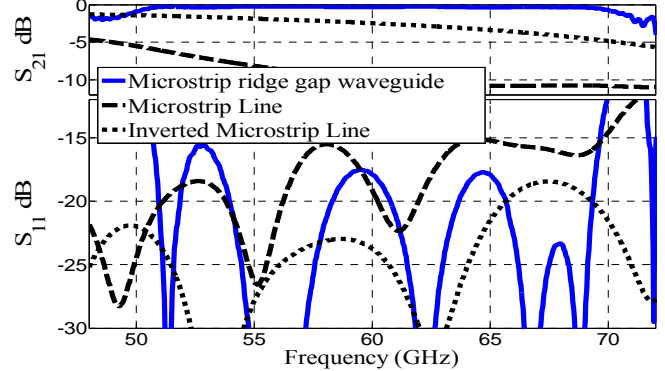


**Figure 15** Simulated  $S_{11}$  and  $S_{21}$  of 2 x 90° bend of microstrip-ridge gap waveguide, microstrip line and inverted microstrip line of similar width, using copper as conductor and RO 3003 as dielectric material.

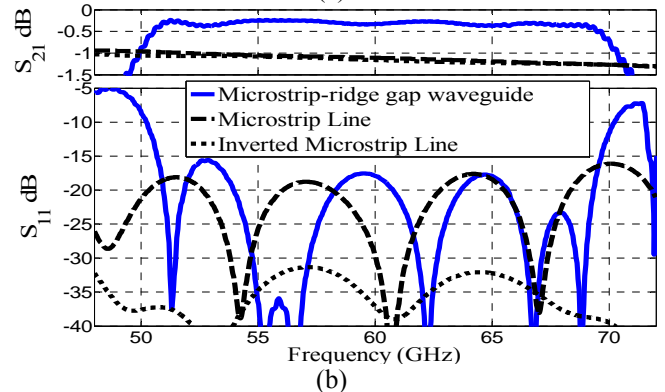
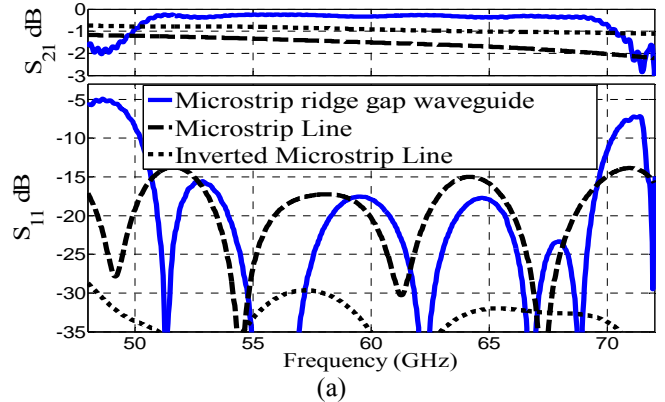


**Figure 16** Simulated  $S_{11}$  and  $S_{21}$  of 2 x 90° bend of microstrip-ridge gap waveguide, microstrip line and inverted microstrip line. (a) The width of the microstrip line and the inverted microstrip line is half of that in Figure 15, using copper as conductor and RO 3003 as dielectric material. (b) The width of the microstrip line and the inverted microstrip line is one quarter of that in Figure 15.

#### IV. DIELECTRIC LOSSES IN MICROSTRIP-RIDGE GAP WAVEGUIDE

In this section we will study the effect of different dielectrics on the transmission losses of microstrip-ridge gap waveguide. For this purpose we have chosen three dielectric materials, i.e., RO3003, RT/duroid 5880 and FR4. The relative permittivity and the loss tangent of each material are summarized in Table 1.

Material	Relative Permittivity	Loss Tangent	Standard thickness used
RT 5880	2.2	0.0009	0.787 mm
RO3003	3.0	0.0013	0.508 mm
FR4	4.7	0.018	0.508 mm

Table 1 Material used for loss comparison.

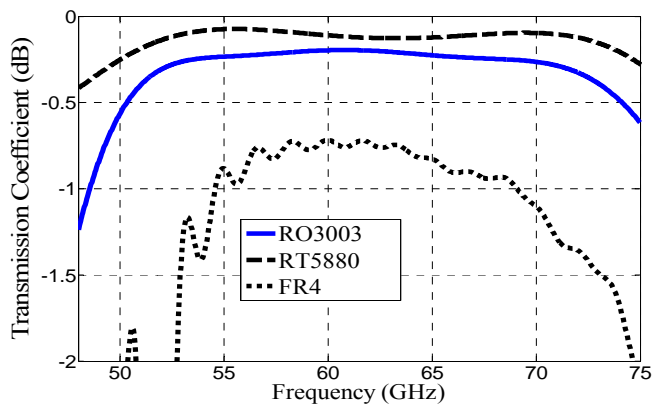


Figure 17 Transmission coefficient of 1.5 cm long microstrip-ridge gap waveguide with different dielectric material.

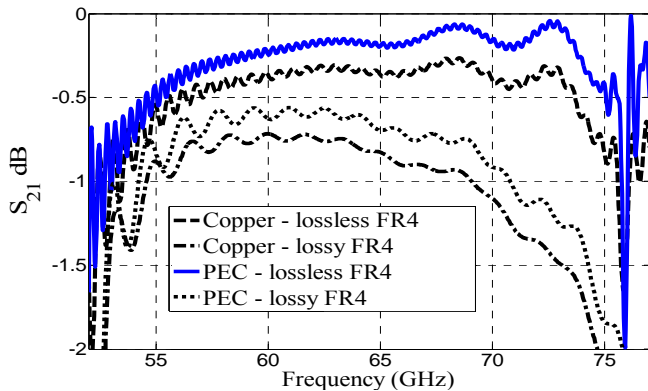


Figure 18 Transmission coefficients of 1.5 cm long microstrip-ridge gap waveguide simulated on FR4 dielectric.

The transmission coefficients, shown in Figure 17, clearly indicate that the losses are larger for larger permittivity as well as loss tangent. Thus, the dielectric has a significant effect on the losses even if we deal with an inverted microstrip-type line having fields mainly in the air gap.

Figure 18 shows the transmission coefficient of microstrip-ridge gap waveguide, using FR4 as the dielectric material. The length of the line is very small, i.e., 1.5 cm, and the width of the line is 1.3 mm.  $S_{21}$  for the lossless material is about -0.2 dB. Unlike the example shown in Figure 14, for microstrip-ridge gap waveguide, the main contributor to the losses in the line is the dielectric material (FR4 is a lossy low cost

material), even though it has wider metal strips. This proves one of the main advantages of using microstrip-ridge gap waveguide: at 60 GHz and above it is possible to make circuits with wider width of the metal strip than for microstrip line and inverted microstrip line, and thereby we significantly reduce the attenuation along the line.

#### V. TRANSITION TO WR-15

Figure 19 shows the basic drawing of the chosen vertical microstrip-ridge gap waveguide to WR-15 transition. The rectangular waveguide is connected from the bottom of the microstrip-ridge gap waveguide. This configuration will enable us to establish a feeding network of an antenna excited via coupling slots in the upper smooth plate as explained in the Introduction. However, the design of it is not straight-forward because we have the planar limitations of the PCB geometry.

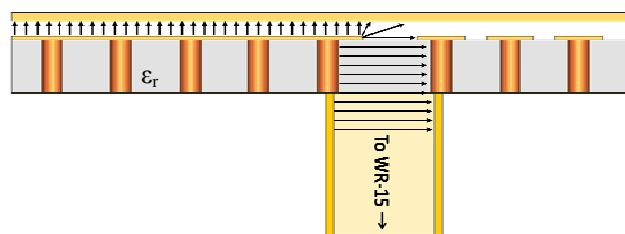


Figure 19 Side view of the basic configuration of the microstrip-ridge gap waveguide to WR-15 transition.

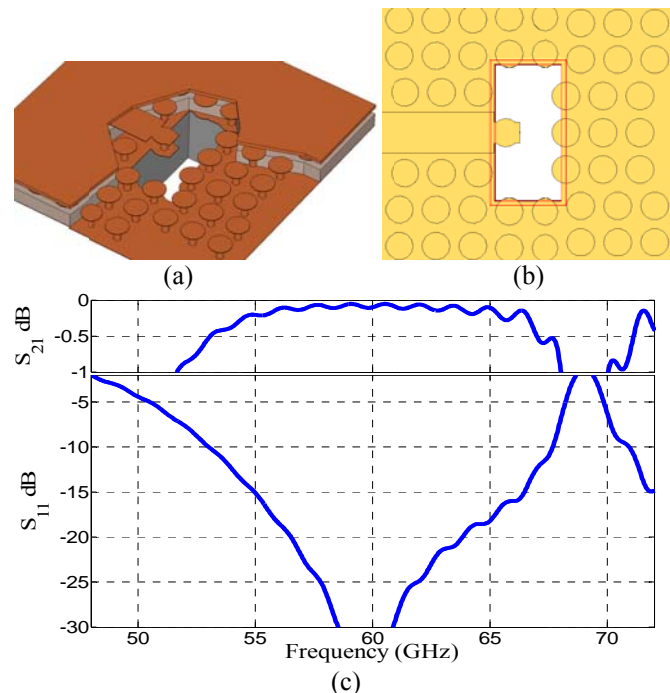


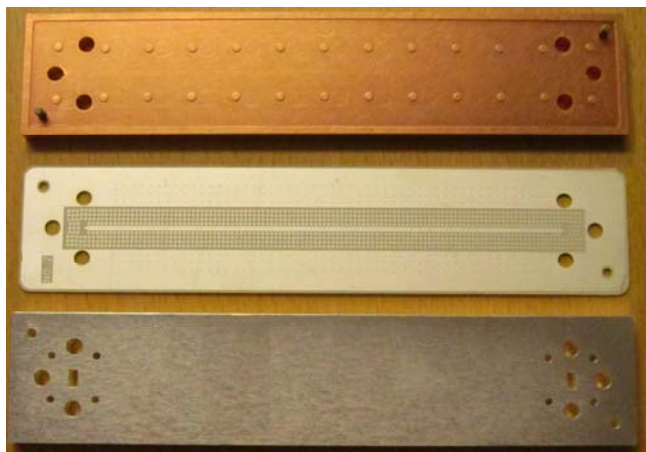
Figure 20 Drawing of the designed transition. a) Side view, b) Top view, c) Simulated S-parameters of single transition.

For this purpose, we make a matching stub at the end of the microstrip-ridge line. This stub is also connected to the ground plane through a via-hole as shown in Figure 20a. By fine-tuning the location of the via-holes around the WR-15 opening, and the width and length of the stub, shown in Figure 20b, we were able to match the microstrip-ridge gap

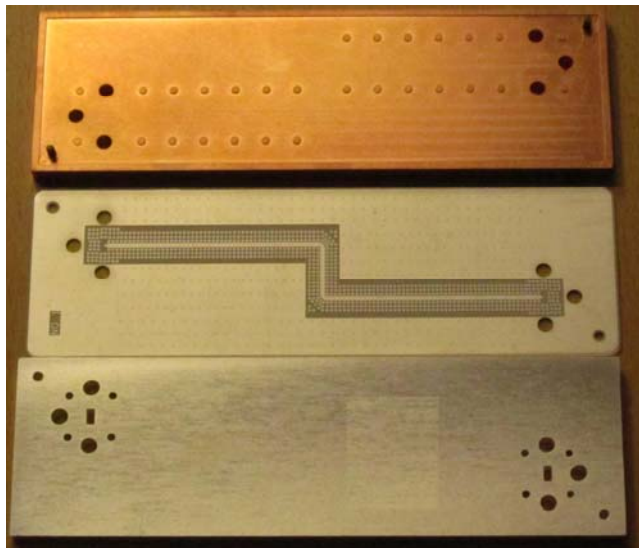
waveguide to WR-15 over the desired bandwidth of 57-66 GHz. The simulated S-parameters are shown in Figure 20c.

## VI. VALIDATION BY MEASUREMENTS

The performances of the 60 GHz microstrip-ridge gap waveguide and its transition to WR15 were validated by S-parameter measurements of some test circuits. Photographs of the test circuits are shown in Figure 21. In the first set of prototypes, the copper lines on the PCBs were unfortunately plated with Electroless nickel immersion gold (ENIG), which is standard for PCBs. This gave very high losses, because of the poor conductivity of nickel. It also caused a shift in the frequency band of  $S_{11}$ . In the second set of prototypes the copper traces were plated with silver. In the selected graphs we show only results for the second set of prototypes.



(a)



(b)

**Figure 21** Photo of the test circuits manufactured. (a) 12 cm long line, (b) 12 cm long with 2 x 90° bend.

### A. Straight section

Figure 22a shows a 12 cm long back-to-back microstrip-ridge gap waveguide to WR-15 transition. The simulated and measured S-parameters (Figure 22b) of the second prototype

show that the reflection coefficient is below -10 dB between 56 and 67 GHz. This would for a low loss line mean that the single transition will be better than -16 dB over this band. However, the measured  $S_{21}$  shows about 0.7 dB more losses than the simulated -1.5 dB over the desired bandwidth. We believe that this difference in transmission coefficient is due to the perturbations of the currents on the microstrip lines caused by the via holes and related surface roughness. During simulation we modeled the upper surface of the microstrip-ridge as smooth copper lines, but in reality it is plated by silver and has a lot of holes in it.

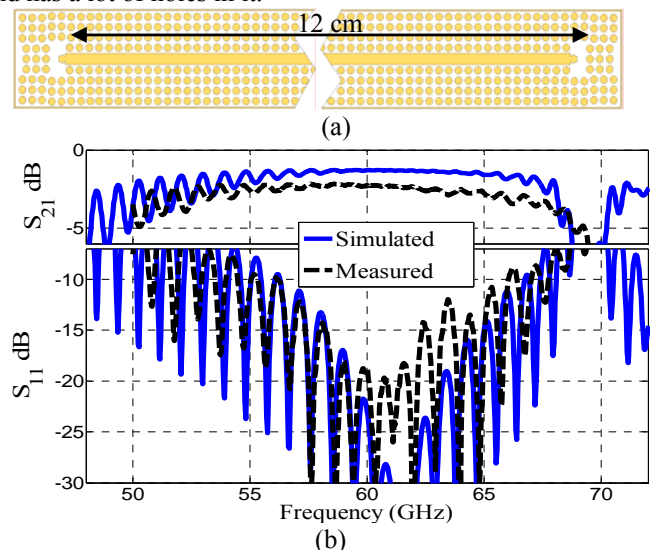


**Figure 22** Microstrip-ridge gap waveguide to WR-15 transition. a) 12 cm back-to-back configuration. b) S-parameters of the structure in a).

The ENIG plating of the first prototype may have very little effect on the conductivity of normal microstrip lines, because then the propagation of the fields is within the dielectric material, so the currents on the microstrip lines are concentrated on their lower surfaces, which are attached to the substrate and contain no ENIG plating (except at the edges of the line). However, in our microstrip-ridge gap waveguide the fields are in the air gap above the substrate and the microstrip line, so that the current on the line will be on the ENIG-plated side of the copper. The transmission coefficient was below -4.2 dB in that case, which is very low compared to the simulated results and the double of the loss in the second prototype without ENIG.

### B. Section with two 90° bends

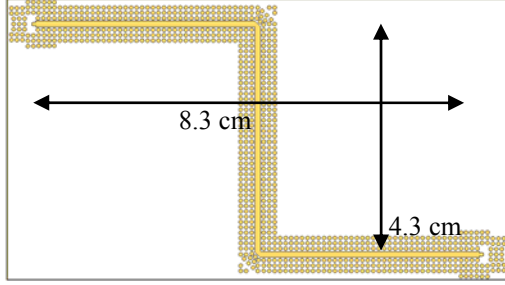
Similarly, we also manufactured microstrip-ridge gap waveguide with two 90° bends and with the same WR15 transitions at both ends. The geometry and simulated and measured S-parameters for the second prototype without the ENIG coating are shown in Figure 23a.

The size of each of the two circuits with 90° bends is 8.3 cm x 4.3 cm, so the path for wave propagation is almost 12 cm long and similar to that we have for the straight line. The simulated and measured  $S_{11}$  is below -10 dB between 56 and 67 GHz, and the simulated transmission coefficient is about -1.5 dB, whereas the measured one is about -2.5 dB. We can

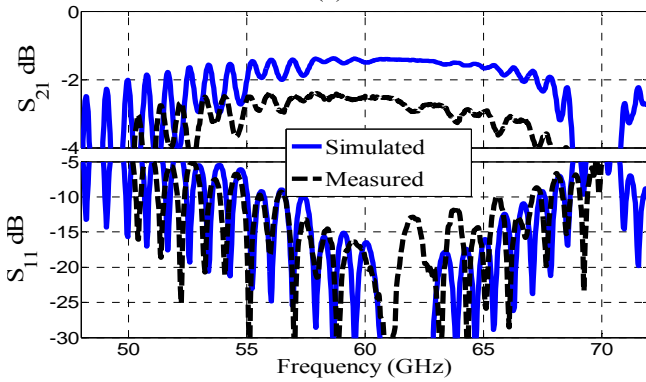
again explain the discrepancy between simulated and measured  $S_{21}$  as an effect of the via holes and related surface roughness.

C. Effect of substrate thickness

The substrates used in Figure 22a and in Figure 23a are 20 mils thick, i.e., 0.508 mm. In order to make circuits more stable and firm, the microstrip-ridge gap waveguide can be made with thicker substrates as well. We have also analyzed the microstrip-ridge and via-hole pins realized on 30 mils (0.76 mm) thick substrate. The most important dimensions of the lines for the two substrate thicknesses are summarized in Table 2.



(a)



(b)

Figure 23 Two 90° bends of microstrip-ridge gap waveguide to WR-15 transition. a) 8.3 cm x 4.3 cm back-to-back configuration. b) S-parameters of the structure.

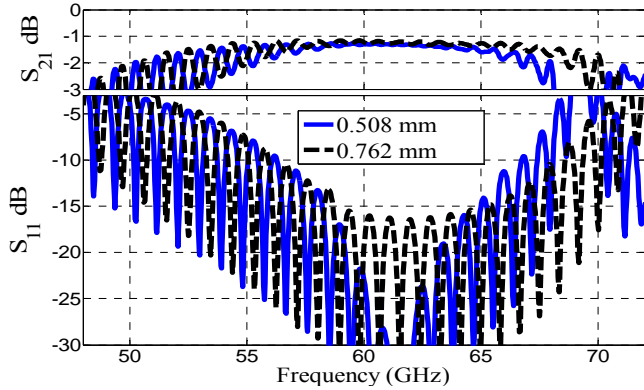


Figure 24 Simulated S-parameters straight microstrip-ridge gap waveguide with back-to-back transition, on 0.508 mm and 0.762 mm thick RO3003 substrates.

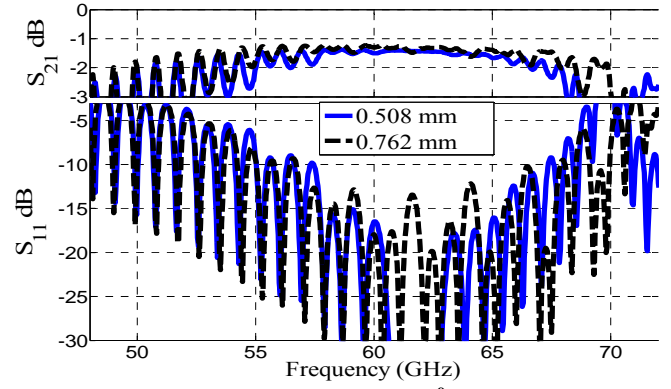


Figure 25 Simulated S-parameters two 90° bends of microstrip-ridge gap waveguide with back-to-back transition, on 0.508 mm and 0.762 mm thick RO3003 substrates.

Parameters	0.508 mm structure	0.762 mm structure
Gap_via	1.0 mm	0.8 mm
D_Pad	0.762 mm	0.559 mm
D_via	0.254 mm	0.254 mm
Gap_Air	0.25 mm	0.25 mm
H_RO3003	0.508 mm	0.762 mm
Line Width	1.1176 mm	1.1176 mm

Table 2 Important parameters of the microstrip-ridge gap waveguide.

Figure 24 shows the simulated S-parameters of both the 0.508 mm and 0.762 mm thick microstrip-ridge straight line of 12 cm length. Although the reflection coefficient is better in the 0.508 mm line, this is slightly lossier than the 0.762 mm line. Similarly, Figure 25 compares the S-parameters of lines with two 90° bends on 0.508 mm and 0.762 mm substrates. The reflection coefficient is better for the 0.508 mm line but again the transmission coefficient is slightly better for the 0.762 mm line case. The lengths of the lines are similar in both cases.

D. Separating the losses in three parts

The total losses in the measured microstrip-ridge gap waveguide circuits are composed of three different parts: the losses in a single transition to WR15 ( $Loss_{Trans}$ ), the losses of a single 90° bend ( $Loss_{bend}$ ), and the losses along the lines themselves. We have also manufactured and measured a short 4cm long straight microstrip-ridge line with back-to-back transitions. The total losses (excluding the mismatch factor) for each of the three cases: short length straight line, 12 cm straight line, and two 90° bend can then be written as

$$Loss_{short\ length} = 2 \times Loss_{Trans} + Line\ loss \times l_{short},$$

$$Loss_{long\ length} = 2 \times Loss_{Trans} + Line\ loss \times l_{long},$$

$$Loss_{2 \times 90^\circ} = 2 \times Loss_{Trans} + Line\ Loss \times l_{bend} + 2 \times Loss_{bend},$$

respectively, where *Line Loss* is the losses per cm of the lines of the three different circuits, and  $l_{short}$ ,  $l_{long}$  and  $l_{bend}$  are the known lengths of the short line, the long line and the line with the two  $90^\circ$  bends, respectively. The three equations with the three unknowns  $Loss_{Trans}$ , *Line Loss* and  $Loss_{bend}$  can easily be solved. The simulated and measured *Line Loss*, which include both dielectric and conductive losses, are shown in the upper part of Figure 26. The simulated *Line Loss* is about 0.09 dB/cm, whereas the measured one is 0.18 dB/cm. Both the simulated and measured losses due to a single transition are about 0.2 dB, and the loss due to single bend is 0.04 dB. We believe that the discrepancy between the simulated and measured line losses is due to surface roughness which include the actual microstructure of the surface of the conductor and the perturbations of the current flow on the microstrip lines caused by the via holes. The simulations are not accurate outside the stopband because there the fields are not bounded by any PMC walls, and, the numerical description of the geometry is incomplete outside the via holes region. This explains the erroneous transmission coefficient there, showing even amplification rather than loss.

For comparison, a rectangular waveguide for 60 GHz was measured to have a loss of 0.04 dB/cm. Similarly, SIW line in a 0.762 mm RO3003 substrate would have a factor 1.3 larger conductive losses due to the smaller dimensions of dielectric-filled waveguides, and additional dielectric losses of 0.1 dB/cm, giving a total of about 0.15 dB/cm. Thus, the losses of SIW lines and microstrip-ridge gap waveguides are comparable.

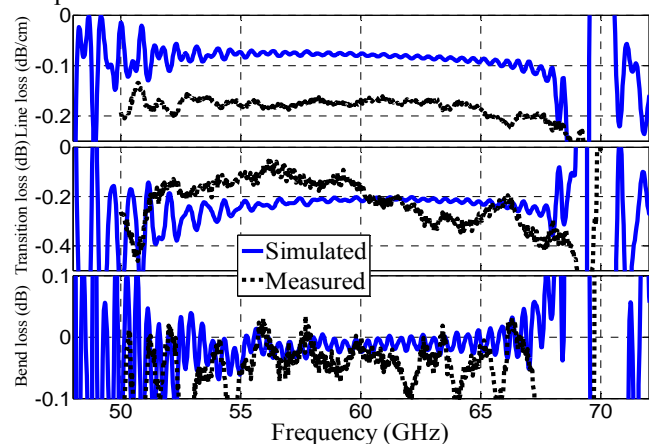


**Figure 26** Losses in Microstrip-ridge gap waveguide which include losses in line (dB/cm) (top plot), losses in transition (dB) (middle plot) and losses at the  $90^\circ$  bend (dB) (bottom plot).

## VII. CONCLUSION

We have done numerical studies and verified experimentally the complete performance of the microstrip-ridge gap waveguide realized in a PCB. The ridge is realized by a metal strip with metalized via-holes, and the AMC pin surface is realized by metalized via-holes with a pad at the top. The latter provide together with the top smooth metal plate the stop band for parallel-plate modes. The results have been compared with the conventional microstrip line and the inverted microstrip line, and we have found that the microstrip-ridge

gap waveguide has lower losses. The reasons are that there is no substrate in the air gap region where the waves propagate, and that we can use much wider metal strip without having problems with radiation and surface waves. We experienced during the work that the reflection coefficient of bends in the line is strongly affected by the position of the via holes closest to the metal strip.

We have also presented a transition from microstrip-ridge gap waveguide to WR-15. This has been verified in a back-to-back configuration with two straight microstrip-ridge gap waveguide lines of different lengths as well as one with two  $90^\circ$  bends. The results show that the reflection coefficient  $S_{11}$  is better than -10 dB over the design bandwidth of 57 – 66 GHz in the back-to-back configuration. The measured transmission losses of the microstrip-ridge gap waveguide is low (0.18 dB/cm), but still about double the simulated losses, which we explain as an effect of the surface roughness and the via holes along the conducting strip. The WR15 transition has a loss of about 0.2 dB, and a  $90^\circ$  bend of 0.04 dB. Finally, we have compared microstrip-ridge gap waveguides realized on substrates of 0.508 mm and 0.762 mm thickness. We found that the 0.762 mm line have slightly lower transmission losses than the 0.508 mm line.

## ACKNOWLEDGMENT

This work has been supported by The Swedish Research Council VR and Pakistan's NESCOM scholarship program. The hardware has been provided by Huawei Technologies Company, China via Huawei Technologies Sweden AB.

## REFERENCES

- [1] P.-S. Kildal, E. Alfonso, A. Valero, and E. Rajo, "Local metamaterial-based waveguides in gaps between parallel metal plates," *IEEE Antennas Wireless Propag. Lett.*, vol. 8, pp. 84–87, 2009.
- [2] P.-S. Kildal, "Three metamaterial-based gap waveguides between parallel metal plates for mm/submm waves," in *Proc. 3rd Eur. Conf. Antennas Propag. (EuCAP 2009)*, 2009, pp. 28–32.
- [3] P.-S. Kildal, A. U.Zaman, E.Rajo-Iglesias, E. Alfonso, and A. V. Nogueira, "Design and experimental verification of ridge gap waveguide in bed of nails for parallel plate mode suppression," *IET Microwaves Antennas Propag.*, vol. 5, no. 3, pp. 262–270, March 2011.
- [4] E. Rajo-Iglesias and P.-S. Kildal, "Numerical studies of bandwidth of parallel plate cut-off realized by bed of nails, corrugations and mushroom-type EBG for use in gap waveguides," *IET Microwaves Antennas Propag.*, vol. 5, no. 3, pp. 282–289, March 2011.
- [5] E. Rajo-Iglesias, A. U. Zaman, and P.-S. Kildal, "Parallel plate cavity mode suppression in microstrip circuit packages using a lid of nails," *IEEE Microw. Wireless Compon. Lett.*, vol. 20, no. 1, pp. 31–33, Dec. 2009.
- [6] A.U. Zaman, T. Vukusic, M. Alexanderson, and P.-S. Kildal, "Gap waveguide PMC packaging for improved isolation of circuit components in high frequency microwave modules," *IEEE Trans. Compon. Packag. Manuf. Technol.*, vol. 4, no. 1, pp. 16–25, 2014.
- [7] A. A. Brazález, A. U. Zaman, and P.-S. Kildal, "Improved microstrip filters using PMC packaging by lid of nails," *IEEE Trans. Compon. Packag. Manuf. Technol.*, vol. 2, no. 7, pp. 1075–1084, July 2012.
- [8] A. Valero-Nogueira, M. Baquero, J. I. Herranz, J. Domenech, E. Alfonso, and A. Vila, "Gap waveguides using a suspended strip on a bed of nails," *IEEE Antennas Wireless Propag. Lett.*, vol. 10, pp. 1006–1009, 2011.
- [9] H. Raza, J. Yang, and P.-S. Kildal, "Study of the characteristic impedance of gap waveguide microstrip line realized with square metal pins," in *Proc. 7th Eur. Conf. Antennas Propag. (EuCAP 2013)*, 2013, pp. 3001–3005.
- [10] S. A. Razavi, P.-S. Kildal, L. Xiang and E. Alfonso, "2×2-slot Element for 60GHz planar array antenna realized on two doubled-sided PCBs

using SIW cavity and EBG-type soft surface fed by microstrip-ridge gap waveguide,” submitted to *IEEE Trans. Antennas Propag.*, Dec. 2013.

- [11] E. Pucci, E. Rajo-Iglesias, J.-L. Vazquez-Roy and P.-S. Kildal, “Planar dual-mode horn array with corporate-feed network in inverted microstrip gap waveguide,” accepted for publication in *IEEE Trans. Antennas Propag.*, March 2014.
- [12] E. Pucci, E. Rajo-Iglesias, and P.-S. Kildal, “New microstrip gap waveguide on mushroom-type EBG for packaging of microwave components,” *IEEE Microw. Wireless Compon. Lett.*, vol. 22, no. 3, pp. 129–131, March 2012.
- [13] H. Raza, J. Yang, P.-S. Kildal, and E. Alfonso, “Resemblance between gap waveguides and hollow waveguides,” *IET Microwaves Antennas Propag.*, vol 7, no. 15, pp. 1221–1227, Dec. 2013.
- [14] CST Microwave Studio (2011), Computer Simulation Technology. [Online]. Available: <http://www.cst.com>.
- [15] Ansoft HFSS (version 12, 2009). [Online]. Available: <http://www.ansoft.com/>.
- [16] E. J. Denlinger, “Losses of microstriplines,” *IEEE Trans. Microw. Theory Techn.*, vol. 28, no. 6, pp. 513–522, 1980.
- [17] R. A. Pucel, D. J. Masse and C. P. Hartwig, “Losses of microstrips,” *IEEE Trans. Microw. Theory Techn.*, vol. 16, no. 6, pp. 342–350, 1968
- [18] R. S. Tomar and P. Bhartia, “Suspended and inverted microstrip design,” *Microwave J.*, vol. 29, no. 3, pp.173–177, March 1986.



**Hasan Raza** received the M.Sc. degree in Engineering in Radio Astronomy and Space Sciences, and PhD degree from the Chalmers University of Technology, Gothenburg, Sweden, in 2007 and 2014, respectively. His research interests include UWB antenna design and gap waveguides.



**Jian Yang** (M’02–SM’10) received the B.S. degree from the Nanjing University of Science and Technology, Nanjing, China, in 1982 and the M.S. degree from the Nanjing Research Center of Electronic Engineering, Nanjing, China, in 1985, both in electrical engineering, and the Swedish Licentiate and Ph.D. degrees from the

Chalmers University of Technology, Gothenburg, Sweden, in 1998 and 2001, respectively.

From 1985 to 1996, he was with the Nanjing Research Institute of Electronics Technology, Nanjing, China, as a Senior Engineer. From 1999 to 2005, he was with the Department of Electromagnetics, Chalmers University of Technology as a Research Engineer. During 2005 and 2006, he was with COMHAT AB as a Senior Engineer. From 2006 to 2010, he was an Assistant Professor, and since 2010, he has been Associate Professor, at the Department of Signals and Systems, Chalmers University of Technology. His research interests include 60–120 GHz antennas, THz antennas, ultra-wideband antennas and UWB feeds for reflector antennas, UWB radar systems, UWB antennas in near-field sensing applications, hat-fed antennas, reflector antennas, radome design, and computational electromagnetics.



**Per-Simon Kildal** (M’82–SM’84–F’95) has been Professor at Chalmers University of Technology, Gothenburg, Sweden since 1989 ([www.kildal.se](http://www.kildal.se)). He has authored antenna textbook, and more than 155 journal articles and letters. Two of these have received best paper awards in IEEE

Transactions on Antennas and Propagation. Kildal has designed the EISCAT VHF antenna and the Gregorian dual-reflector feed of the radiotelescope in Arecibo. He has invented several reflector antennas and feeds, such as the hat feed and the eleven feed. Kildal is the originator of the concepts of soft and hard surfaces, and gap waveguides. Kildal’s research group has pioneered the reverberation chamber into an accurate tool for OTA-characterization of wireless devices subject to Rayleigh fading. Kildal received the Distinguished Achievements Award of the IEEE Antennas and Propagation Society in 2011.



**Esperanza Alfonso Alós** received the M.S. and Ph.D. degrees in electrical engineering from the Universidad Politécnica de Valencia, Valencia, Spain, in 2004 and 2011, respectively.

From 2004 to 2010, she was a Research Assistant at the Institute of Telecommunications and Multimedia Applications (iTEAM), Universidad Politécnica de Valencia. She was a Postdoc Researcher in Antenna Systems at Chalmers University of Technology, Gothenburg, Sweden, from 2011 to 2013, where she was contributing to the development of microwave passive devices and mm-wave antennas in gap waveguide technology. She is currently a Senior Antenna Designer at Gapwaves AB, Gothenburg, Sweden. Her research interests includes computational electromagnetics, antenna design and gap waveguides.